

Australian Winter Storms Experiment (AWSE) I: Supercooled Liquid Water and Precipitation-Enhancement Opportunities

ALEXIS B. LONG*** AND ARLEN W. HUGGINS**

* *Division of Atmospheric Research, CSIRO, Aspendale, Victoria, Australia*

** *Atmospheric Sciences Center, Desert Research Institute, Reno, Nevada*

(Manuscript received 9 October 1990, in final form 10 November 1991)

ABSTRACT

Some results of the first (1988) Australian Winter Storms Experiment are described. The results shed light on precipitation-enhancement opportunities in winter cyclonic storms interacting with the Great Dividing Range of southeast Australia. The results come from analysis of supercooled liquid water amounts provided by a dual-wavelength microwave radiometer, atmospheric structure from Omegasondes, and precipitation amounts from a large number of tipping-bucket gauges. With these data it is possible to calculate and compare two of the terms in a condensed-phase water budget over a cloud-seeding target area in the Great Dividing Range. The two terms are the horizontal flux of supercooled liquid cloud water entering the budget volume and the vertical precipitation flux at ground level out of the volume. The budget terms have implications for the amount of extra precipitation that may result from seeding. It is found that the amount depends on the frontal or postfrontal stage of activity in the target area and on the wind direction with respect to the mountainous terrain.

1. Introduction

The Commonwealth Scientific and Industrial Research Organization (CSIRO) Division of Atmospheric Research is advising the Melbourne and Metropolitan Board of Works (MMBW) in Australia on its ongoing 5-yr randomized cloud-seeding experiment. The broad aim of the experiment is to learn by how much and under what circumstances precipitation can be enhanced over Melbourne's main Thomson Reservoir water-supply catchment (Fig. 1). The experiment specifically aims to show whether wintertime (May–October) precipitation over the catchment target area can be increased by upwind aircraft cloud seeding with silver iodide or dry ice, at cloud-top temperatures colder or warmer than -7°C , respectively [See Long and Shaw (1988)].

The Australian Winter Storms Experiment (henceforth, known as AWSE) is a research program that is being conducted by CSIRO alongside the MMBW cloud-seeding experiment on a noninterference basis. The Desert Research Institute (DRI) is cooperating with CSIRO in AWSE. One purpose of AWSE is to increase knowledge of the clouds in the vicinity of the cloud-seeding target area in order to increase understanding of the cloud-seeding experiment. As an additional benefit, AWSE is also expected to identify seeding opportunities not included in the present MMBW experiment.

Phase I of AWSE was conducted in July and August 1988. The objectives of AWSE I were the following.

(i) Determine the horizontal supercooled liquid water flux in clouds over Baw Baw Plateau (Fig. 1) and compare it to the vertical precipitation flux in the target area.

(ii) Determine the meteorological circumstances under which large fluxes of supercooled liquid water are present.

(iii) Develop an understanding of the microphysical and other limitations on the natural precipitation processes.

(iv) Devise a hypothesis as to how the limitations can be overcome by cloud seeding and how practical, significant precipitation increases can be produced.

(v) Test the proposed seeding hypothesis, physically and statistically, in a future field experiment.

The purpose of the present paper is to describe and discuss advances made toward objectives (i) and (ii) through the analysis of three AWSE storms sampled in 1988.

The physical situation envisioned in this paper is as follows and is similar to that in Heggli (1986), Boe and Super (1986), Thompson and Super (1987), and Super and Boe (1988a). On the upwind side of rising orography, oriented roughly northwest–southeast in this article, there are midlatitude westerlies. The westerlies carry moist air up and over the western slopes of the orography, and clouds form. Some precipitation develops in, and falls from, the clouds.

At any point on the mountain slope, including the

Corresponding author address: Dr. Alexis B. Long, Division of Atmospheric Research, CSIRO, Private Bag No. 1, Mordialloc, Victoria 3195, Australia.

crest, a westerly supercooled liquid water flux can be defined. A fraction of the flux will be naturally unused in the precipitation processes and will be unconverted to ice particles or precipitation. This fraction has been termed "excess flux" (Thompson and Super 1987) or "nature's surplus water" (Super and Boe 1988a). The flux will be present in the flow over the crest and down the lee side of the orography. There the supercooled liquid water will evaporate. An estimate of the unused supercooled liquid water flux near the crest will serve as a useful upper bound on the potential additional precipitation that may come from cloud-seeding upwind. The amount of additional precipitation in a given case will depend on precisely where the seeding is done, on the seeding material, on the distribution of supercooled liquid water, on the cloud microphysics, and on the cloud dynamics.

The estimate of the supercooled liquid water flux at the crest is usefully compared, in the kind of analysis to be done here, with the runoff over a nearby river basin or with the precipitation over a nearby land area. If the river basin is on the upwind side of the orography (and descending to the west, for example), then the ratio of flux to runoff is a measure of how much the runoff may be fractionally increased by seeding the clouds above the upwind part of the orography. If the precipitation area is on the downwind side of the crest of the orography (east, for example), then the ratio of flux to precipitation is a measure of how much the precipitation may be increased by seeding the clouds above the upwind part of the orography. In a given case, the seeding will tend to increase the runoff or precipitation more on one side of the mountain crest than on the other, depending on where seeding and supercooled liquid water are located. If the water is near the mountain crest, for example, then there will be a greater likelihood that the additional precipitation (should it eventuate) will fall downwind of the crest, and the flux will be an upper bound on this additional precipitation.

Some ratios of supercooled liquid water flux to runoff or precipitation can be quoted. Heggli (1986) calculated the flux from radiometer liquid water data collected near the head of the westward-flowing American River basin in California and from a mean downwind speed of the water. Over three and a half months, from 1984–85, he calculated 2.3×10^5 MI of liquid water escaping the basin downwind (approximately east). (It should be noted that here and elsewhere the numbers quoted by the mentioned authors are rounded off to two significant figures.) This was to be compared to 1.9×10^6 MI of runoff from the basin throughout the 1984–85 July–June water year. The ratio of 0.12 of the two figures provides an upper bound on the increase in runoff that might have occurred with seeding during the period of liquid water measurements. Using radiometer data and wind-speed data from a 70-m-high tower, Boe and Super (1986) calculated 130 mm (pre-

cipitation equivalent) of supercooled liquid water flux. This was compared with 280 mm of actual precipitation on the Grand Mesa in Colorado. The 0.46 fractional ratio is an upper bound on how much the precipitation might have been increased by seeding. (These results were for a 5-month period from 1983 to 1985.) Rauber and Grant (1987) compared the flux of 6.2×10^3 MI from one 2-day winter storm in 1983, calculated from radiometer data, from the "normal wind component at crest height," and from the mountain crest length, against the mean seasonal runoff of 4.7×10^4 MI from the Tushar Mountains near Beaver, Utah. The ratio is 0.13 and represents the fractional increase in runoff that could potentially occur by seeding a major winter storm upwind of the mountains. Finally, near the Mogollon Rim of Arizona, Super and Boe (1988a) observed 3.7×10^4 MI of supercooled liquid water flux over a 2-month period from a radiometer and a variety of wind-measuring instrumentation. The climatological mean annual runoff from the same area was 7.8×10^4 MI. The ratio of the two figures is 0.47 and represents the potential fractional increase of runoff that might develop from seeding.

Although fractional potential increases in precipitation or runoff that might have come from seeding have come from the above studies, these figures are preliminary. The wind speeds that have been used in calculating the supercooled liquid water flux have too often simply been constant values—both as a function of time and as a function of altitude. Super and Boe (1988a) have considered these dependences, but improvements are still needed, perhaps by obtaining and considering frequent sonde data collected throughout storms.

Although runoff data have been used in some of the above studies, precipitation data can and ought to be used more. The long averaging time of runoff data (of days–weeks–months), the dependence of runoff on the size of the catchment, the catchment slope, the kind of vegetation, soil, and rock, and whether rain or snow has fallen reduce the comparability of the runoff data with the frequently short-term supercooled liquid water flux, except in those cases where the liquid water flux is deliberately averaged over the long term. Precipitation amounts, on the other hand, are more temporally compatible with the fundamental unaveraged supercooled liquid water fluxes, especially over short-term periods of hours. These ideas suggest that future studies of the potential precipitation from seeding make more use of precipitation data. The precipitation data will naturally be improved by using a relatively dense network of high-resolution gauges.

2. Instrumentation and data collection

In AWSE I focus was placed on clouds and precipitation in the vicinity of Baw Baw Plateau (1500-m

MSL altitude). [Average elevation of the target area (Fig. 1) is 780 m MSL.] This plateau serves as part of the southwest boundary of the target area (see Fig. 1). For southwesterlies the plateau provides continuing uplift of approaching moist air and promotes orographic development of clouds containing significant supercooled liquid water.

Although water substance is processed by the cloud over the plateau relatively quickly (tens of minutes), the lifetime of the cloud can be tens of hours. In view of this, and given the presence of terrain embedded

within the clouds, a decision was made to sample the clouds with remote-sensing methods primarily. Aircraft sampling above the terrain occurred but only in clearly safe flying conditions and then to sample the clouds at places not covered for the most part by the remote-sensing instrumentation.

Data were collected by the various instrumentation either (a) to fulfill the function of research support for core studies of cloud and precipitation (discussed below) or (b) as part of the core cloud and precipitation studies themselves.

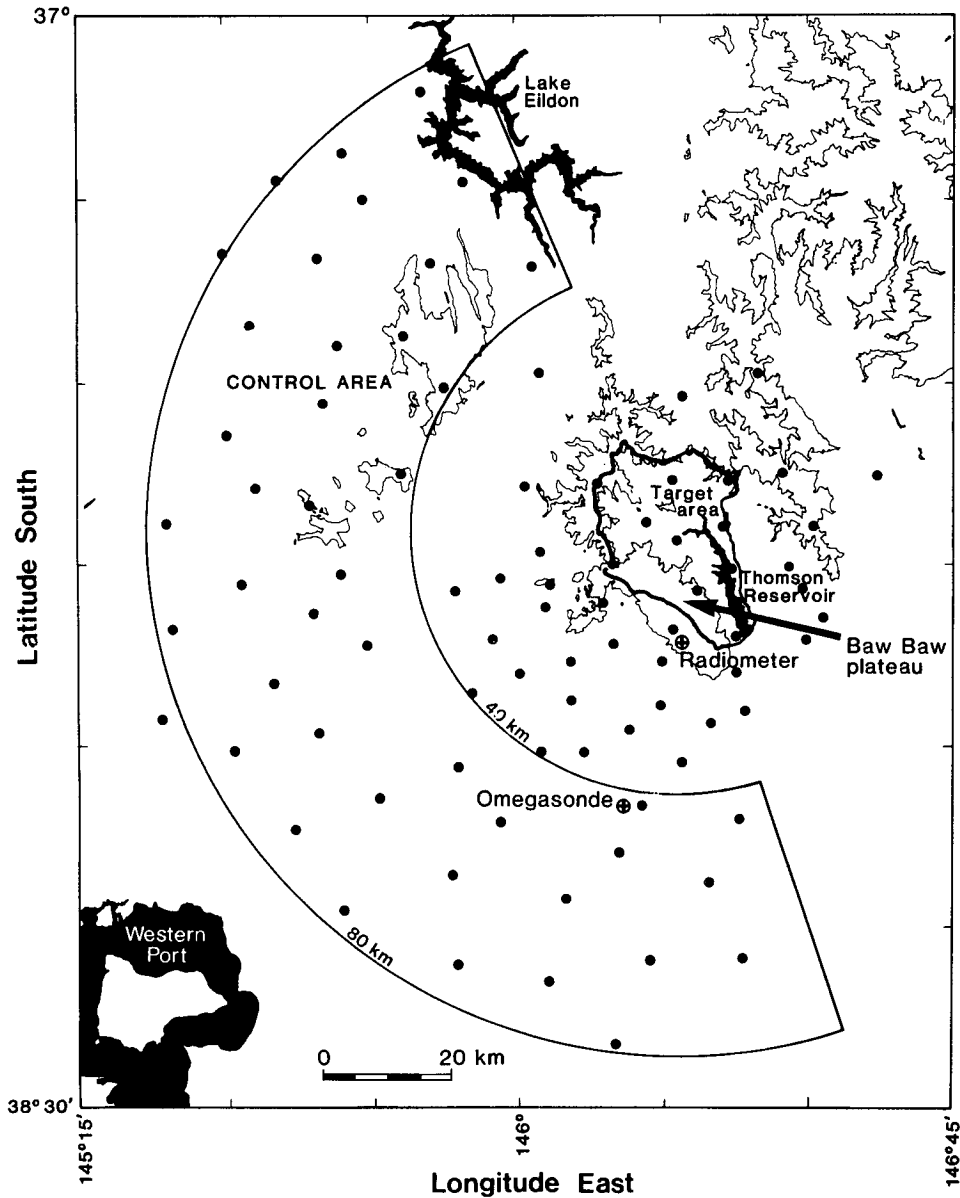


FIG. 1. Map showing 1000-m contour of Great Dividing Range east of Melbourne, outline of target (catchment) area of MMBW cloud-seeding experiment, outline of control area, Thomson Reservoir and Baw Baw Plateau, positions of 87 precipitation gauges, and positions of radiometer and Omegasonde.

a. Research support

Data-collection activities in this category occurred every day and were associated with the infrastructure of the simultaneous MMBW precipitation-enhancement experiment. Described here are the research-support precipitation measurements.

A total of 87 tipping-bucket gauges were placed in the field to record the precipitation on data loggers (Fig. 1). Of these gauges, 10 were in the target area of the MMBW precipitation enhancement experiment and 45 were in the semiannular upwind control area. A total of 17 gauges were placed around the target area and between it and the control area in order to fill in the precipitation field. An additional 15 supplementary gauges were placed in the field, especially for AWSE I, to gather detailed precipitation information near Baw Baw Plateau. Each gauge was sited in an area such that obstructions were beneath a line of 45° elevation angle drawn from the top of the gauge. The gauges were not equipped with windshields. All gauges above the 800-m elevation were equipped with internal liquified petroleum gas heaters to melt any snow and to permit the tipping-bucket mechanism to work. Wind speeds at the gauge orifice during a storm were not measured, but it is estimated they were about 10 m s^{-1} . Overall, the gauges were 95% reliable and provided high temporal accuracy ($\sim 2 \text{ min}$) and high accuracy ($\sim 2\%$) with respect to amount. The latter accuracy applies to measurements of precipitation amounts that have already entered a gauge.

b. Core studies of cloud and precipitation

The core studies in AWSE I focused on winter storm periods when significant cloud cover and precipitation were present in the experimental area. During these periods the following instruments or observation systems were operated. [The CSIRO Office of Space Science and Application (COSSA) F-27 cloud-physics aircraft was also operated, but its data will be discussed in a separate paper.]

1) OMEGASONDES

Important information came from Vaisala/Digicora Omegasondes launched at Blue Rock Reservoir (Fig. 1) by the Bureau of Meteorology. The sondes usually were launched near the beginning of a storm and, thereafter, every 3 h, or sometimes 6 h, until the storm ended. Sondes typically collected data up to the 120-mb level. Raw and derived data variables included equivalent potential temperature, wind speed and direction, temperature, and dewpoint depression. The Omegasonde data, rather than the synoptic data, are used in the meteorological analysis in this paper.

2) RADIOMETER

The Desert Research Institute operated a dual-wavelength ($\lambda_1 = 1.46 \text{ cm}$, $\nu_1 = 20.6 \text{ GHz}$, and λ_2

$= 0.95 \text{ cm}$, $\nu_2 = 31.6 \text{ GHz}$) steerable microwave radiometer (Hogg et al. 1983). The radiometer was located on Baw Baw Plateau (Fig. 1). The longer wavelength (lower frequency) is primarily sensitive to the condensed "depth" of water vapor integrated through the extent of the atmosphere along the viewing direction. (When this depth is adjusted for any slant path it is the same as the precipitable water.) The shorter wavelength (higher frequency) is primarily sensitive to the integrated amount of liquid water in the viewing direction. The field of view of the radiometer is 2.5° wide.

The radiometer collected data in zenith and azimuth-scan modes. In the more common zenith mode the radiometer was pointed vertically and gathered information on temporal Eulerian changes in the integrated depth of liquid water in the cloud passing overhead. In the less common azimuth-scan mode the radiometer was pointed toward a fixed angle above the horizon and steered through 360° of azimuth at a rate of 0.5° s^{-1} . (The scan rate was limited by the time constant of the instrument.) Information was thereby collected on the spatial distribution of liquid water in the atmosphere.

3. Quality of radiometer data

The quality of the radiometer data can be judged 1) by comparing the data with data from an independent instrument to arrive at a measure of the accuracy of the radiometer and 2) by considering how frequently the radiometer data warrant confidence and are "good" rather than "bad."

The accuracy of the radiometer can be judged from a comparison of the integrated vapor depth, as measured with the radiometer, with the depth as measured with the project Omegasondes. The radiometer measures the depth above its site elevation (1500 m MSL) on Baw Baw Plateau. The sonde depth comes from downward integration of the absolute humidity from the top of the sounding to the same 1500-m MSL elevation. Figure 2 compares the two kinds of measurements for the three winter storms discussed in this paper. The discrepancy between the measurements is due in part to errors in both instruments and in part to differences in the sampled parts of the atmosphere. The two kinds of measurements (in cloud as shown here) are only $\sim 0.1\text{--}0.2 \text{ cm}$ apart. This is of the same order of magnitude as found by Hogg et al. (1983) with the National Oceanic and Atmospheric Administration (NOAA) Wave Propagation Laboratory radiometer.

The radiometer data required editing due to several problems. Faulty electronic components and radio-transmission interference produced easily recognized "spikes" in the liquid and vapor depth traces. These "spikes" were deleted and accounted for data losses of 0.7%, 3.2%, and 0.0% of the total durations of the three case-study storms. For periods when rain, drizzle, or melting snow were suspected of contributing to the

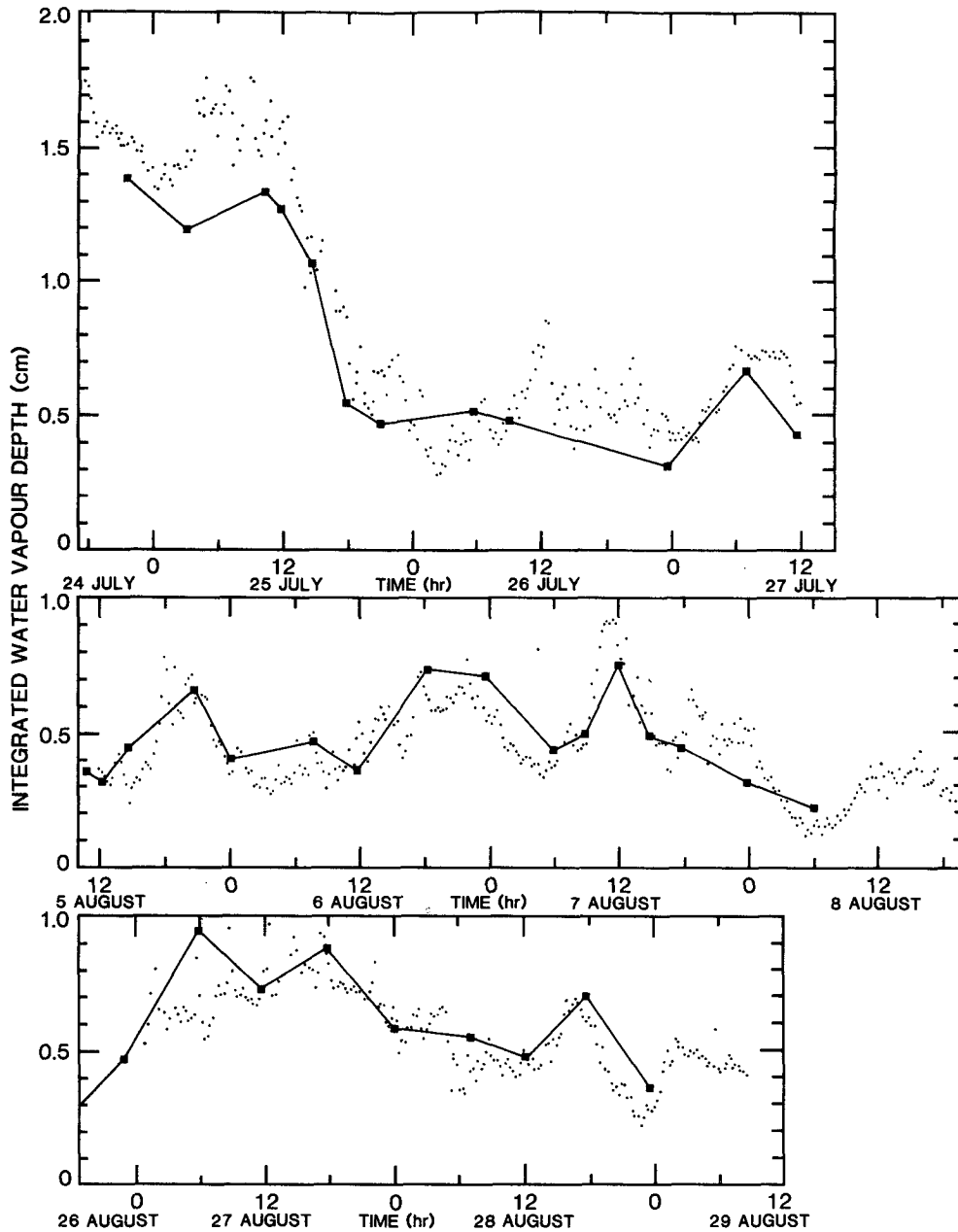


FIG. 2. Comparison of the three storms considered in this paper of the path integral of water vapor from the top of the atmosphere down to the 1500-m altitude of the radiometer site, as measured by the radiometer (dots) and by the OmegaSonde (solid squares connected by line segments).

received signal by extra emissions and/or scattering (identified by weather observations and the tendency of both liquid and vapor to increase markedly), the data were deleted from the set. At times, usually when the outside air temperature was near freezing, a buildup of wet snow occurred at the center of the spinning reflector, causing abnormally high vapor and liquid readings. Operator observations and vapor and liquid tendencies allowed these periods to be edited from the dataset. In all, precipitation-related problems ac-

counted for data losses of 0.4%, 2.4%, and 2.4% for the three storm periods.

The quality of the radiometer data was also dependent on how much data were collected with a temperature T_r of the radiometer that was greater than or less than 0°C . A significant fraction, 38.5 h or 23%, of the three-storm data was collected in conditions of $T_r > 0^\circ\text{C}$. (See marked time intervals with $T_r > 0^\circ\text{C}$ in Figs. 5, 7, and 8.) With these temperatures it is not clear what fraction of the liquid water in the clouds

overhead is at temperatures greater than 0°C and what fraction is supercooled at temperatures less than 0°C . Complete assurance that there is some *supercooled* liquid water, which is necessary for glaciogenic cloud seeding, only comes with $T_r < 0^{\circ}\text{C}$. Such temperatures occurred 77% of the time in the three storms being studied here. This is sufficient to support the conclusions in this paper.

4. Condensed-phase water-budget components

The approach to be taken in the data analysis and interpretation can be understood from Fig. 3. This shows a schematic cross section through the clouds reaching to cloud top. The cross section is upwind and downwind of Baw Baw Plateau. (See Fig. 1 for the location of the 1000-m MSL contour.) The schematic position of the radiometer near the crest of Baw Baw Plateau as used in 1988 is shown in Fig. 3. Typical positions of the precipitation gauges and of the Omega-sonde are shown.

Two components of the *condensed-phase* water budget for the cloud volumes upwind and downwind of the plateau are of interest. There are other components, but they are not of interest in the present study. The components cover broader ranges of particle types and sizes than would be used in a numerical model of

cloud and precipitation processes. One component is a_2 , the horizontal flux of supercooled *cloud* liquid water mass, into the downwind cloudy volume 2, integrated over the upwind end of the volume. It is important to note that a_2 refers to *supercooled* cloud liquid water. This kind of liquid water, as opposed to rain, drizzle, or wet or melting snow or liquid water warmer than 0°C , is important for precipitation enhancement by glaciogenic seeding. The component d_2 is the precipitation mass flux downward out of the downwind cloudy volume, integrated over the ground surface. The integrated ground surface area for the downwind volume is assumed to be the size of the target area used in the seeding experiment.

From the standpoint of cloud-seeding potential an important study is of a_2 and d_2 . By comparing the magnitudes of these terms during winter storms it should be possible to identify the time period of a potential increase of precipitation from seeding and a fractional measure (a_2/d_2) of that increase.

5. Water flux calculations and interpretation

The budget components d_2 and a_2 can be calculated from the precipitation gauge, radiometer, and Omega-sonde data.

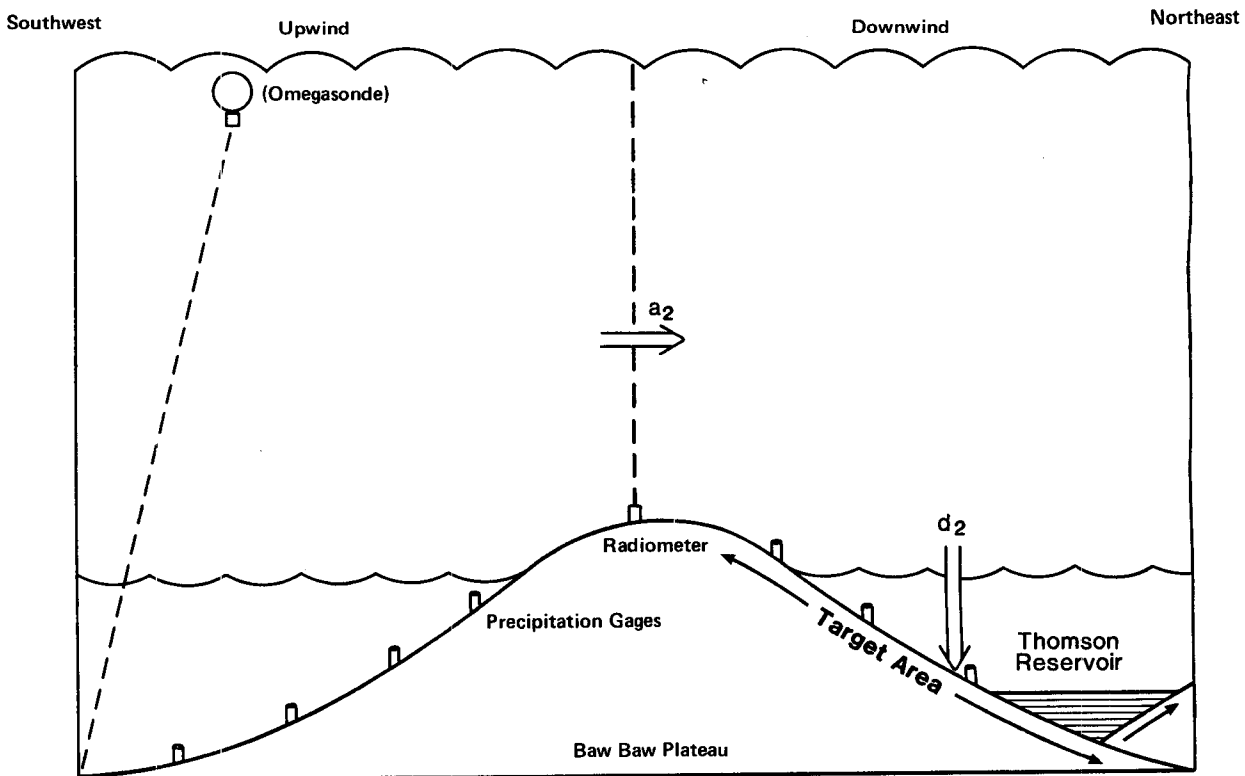


FIG. 3. Schematic vertical cross section through a cloud upwind, over, and downwind of Baw Baw Plateau or other mountain ridge on the west side of the target area. The labeled fluxes are condensed-phase water-budget components, across and downward, downwind of the plateau.

The vertical precipitation flux comes from the formula

$$d_2 \text{ (MI h}^{-1}\text{)} = \frac{1}{10} \sum_{i=1}^{10} r_i \text{ (mm h}^{-1}\text{)} A \text{ (km}^2\text{)}, \quad (1)$$

where r_i is the precipitation rate at the surface at the i th of ten gauges in the target area. The area A of the target area is 487 km². An average precipitation of 1 mm melted depth over the target area amounts to 487 MI. [For reference, 1 MI (megaliter) is equal to 0.8107 acre-ft.]

The error in estimating d_2 in the left-hand side of (1) depends on the error in the average precipitation rate measured with the ten gauges placed in the target area. If the error at each of these gauges is 50% in 15 min, as proposed by a reviewer, then the average error over ten gauges should be smaller by a factor of about 10^{1/2} (Fraser 1958). We, therefore, estimate the error in d_2 to be about 20% over a 15-min period. These error estimates do not allow for systematic undercatch by a group of gauges in windy conditions.

The horizontal supercooled liquid water flux comes from the formula

$$a_2 \text{ (MI h}^{-1}\text{)} = 3.6W \text{ (mm)} \bar{V} \text{ (m s}^{-1}\text{)} \bar{d} \text{ (km)}. \quad (2)$$

At a given time, the flux a_2 is estimated at the intersection point of 1) the ridge crest along the upwind boundary of the target area and 2) a line parallel to the wind direction within the cloud and extending upwind from the center of the target area to the point where it intersects the boundary ridge crest. This intersection point is called the upwind boundary point or simply the boundary point (Fig. 4). It is on the upwind side of the downwind budget volume. Both the boundary point and the budget volume rotate about the center of the target area as the wind direction varies.

In (2), W is the depth of supercooled liquid water integrated from the radiometer altitude on Baw Baw Plateau to cloud top. The wind speed \bar{V} is the length of the mean wind-velocity vector measured over several altitudes. The altitudes are separated by 10 mb and extend from the radiometer pressure altitude of 840 mb up to either the cloud top or the -15°C level, whichever is lower. The cloud top is defined by a dew-point depression of 3°C. At this depression, the relative humidity is 79% ± 2% for temperatures in the range of 0° to -20°C and pressure is in the range of 600–800 mb. The -15°C limit is similar to the -15°C cold limit on cloud tops presented in the conceptual models of Rauber and Grant (1986) for supercooled liquid water distribution in clouds near mountains. Similar cold-temperature limits for supercooled liquid water were observed by Super and Heimbach (1988) and Super and Boe (1988b). In (2) no provision is made for the supercooled liquid water being concentrated at a particular height. This is demonstrated by the several wind velocities at equal-pressure height intervals that go into the calculations of \bar{V} . The variable \bar{d} in (2) is the average width of the target area perpendicular to the line described in aforementioned item 2. Typically,

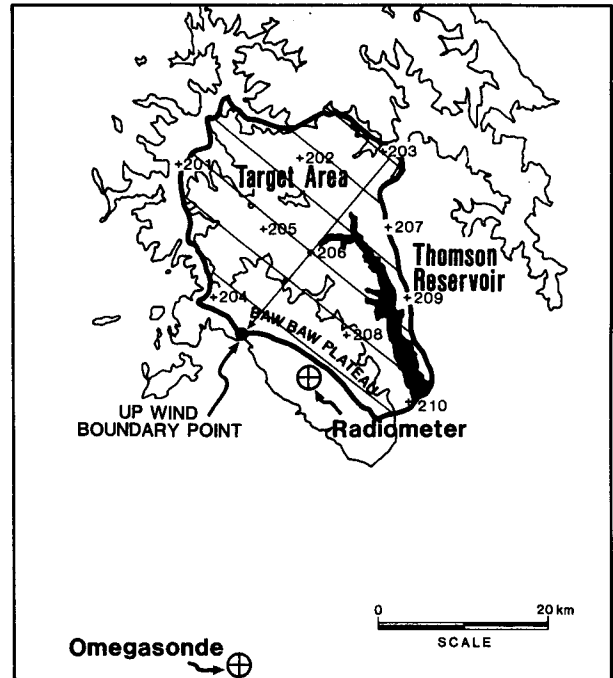


FIG. 4. Diagram showing how the average width of target area \bar{d} is calculated. This diagram is for a wind direction of 220°. The upwind boundary point is at the intersection of the line extending from the target-area center point (at +206 precipitation gauge location) along azimuth 220° to the large boldface dot on the boundary line of the target area. The backward extension of the line from the center point is also drawn. Lines perpendicular to the 40°–220° line and every 4 km apart are drawn. The average length \bar{d} of these lines is calculated, and this is the average width of the target area for an azimuth of 220°.

seven values for the width at various distances downwind from the boundary point are measured at any time and then averaged (see Fig. 4).

For (2) the “errors” in the constituent terms making up a_2 are about 10% for W , 15% for \bar{V} , and 20% for \bar{d} . Heggli et al. (1987) have examined how closely two radiometers, similar to the one used in the present project, agreed over several months of 1984–85. The rms difference in the liquid water depth was 0.02 mm. This amounts to a relative difference of 10% or less for liquid water depths of 0.2 mm or greater. A liquid depth of 0.3–0.5 mm was observed in the three storms treated here in Figs. 5, 7, and 9. The errors in Omegasonde vector winds are 2–3 m s⁻¹ according to the Australian Bureau of Meteorology for vector winds and less for wind speeds alone. This suggests a 13%–20% error in wind speed for a 15 m s⁻¹ wind speed. A typical error in \bar{d} can be derived from Fig. 4. It shows six transects across the target, the lengths of which are averaged to estimate the mean width \bar{d} . The sample standard deviation in the individual lengths is 10 km, and the deviation in their mean is 4 km. Inasmuch as the mean width is 20 km, the mean error in \bar{d} is about 20%.

The errors in W and \bar{V} apply, respectively, at the radiometer location where W is measured and at the horizontal and vertical location of the Omegasonde

balloon where \bar{V} is measured. There is an additional error in extrapolation of W and \bar{V} from their respective measurement locations to the boundary point. The extrapolation error will depend on the distances between these measurement locations and the boundary point that in turn will depend on the wind direction. No attempt has been made to evaluate the extrapolation error for \bar{V} , but the factors influencing this error in W have been identified as follows.

The error in estimating W at the boundary point from W at the radiometer site depends on several factors at each location. The factors are the wind velocity directed toward the upwind terrain, the altitude, slope, and shape of the upwind terrain, the upward motions in cloud, the total lift of moist air through the clouds, and the resulting condensation of supercooled liquid water in the clouds. These factors will naturally converge toward each other as the distance between the boundary point and radiometer site decreases. The result will be a reduced error in estimating W .

These general ideas allow us to infer the particular circumstances under which an accurate estimate of a_2 at the boundary point is obtainable from the available radiometer data. These circumstances are classified according to whether the wind aloft and directed toward the terrain is northwesterly or southwesterly. Such northwesterly and southwesterly winds are commonly observed in the frontal and postfrontal stages, respectively, of winter storms in the study area.

a. Northwesterly wind

In this case the boundary point is about 30 km north-northwest of the radiometer site and relatively far away along the boundary ridge. The wind impacts the north-west boundary of the target area, approximately orthogonally, and there is lift up and over the ridge. At the radiometer site and the adjacent Baw Baw Plateau, however, the northwesterly wind would be parallel to most of the terrain contours; the terrain slope will be shallow for the northwesterly wind; there will be a minimum lift at the radiometer site; and the air will be expected largely to go around the plateau rather than over it. Observations show cloud development only over the initial terrain rise at the northwest "nose" of the plateau. Overall, a lower amount of supercooled liquid water would be hypothesized at the radiometer than upwind at the boundary point where the main wind-induced lift occurs. This suggests that a_2 extrapolated to the boundary point from the radiometer at its actual site will be an underestimate of a_2 , which could have been measured with the radiometer at the boundary point.

b. Southwesterly wind

With this wind, the boundary point and radiometer are only about 9 km apart along the southwest side of the plateau. Because of their close separation, the two sites will be in the same region of southwest winds per-

pendicular to most of the contours of Baw Baw Plateau. The winds are expected to be lifted over the plateau orography at both sites rather than go around it. There will also be condensation and liquid water development aloft. Overall, a_2 should have a similar value at the two sites. The estimate by the radiometer of a_2 at the boundary point should be good.

The overall conclusion is that the supercooled liquid-water flux a_2 should be *underestimated* for clouds in the present study when the wind is northwesterly. For southwesterly winds, however, the flux should be better estimated.

The next three sections (6, 7, and 8) describe three storms from 1988. The ideas of the present section 5 are used to support the conclusions drawn in these sections.

6. Storm 1: 5–8 August 1988

This section discusses the supercooled liquid water and precipitation fluxes for storm 1, and their relation to the local atmospheric structure.

Figure 5 shows the precipitation flux and two supercooled liquid water variables. The magnitude of the precipitation flux d_2 (defined in sections 4 and 5) is shown in the hatched histogram in the bottom panel. The supercooled liquid water flux a_2 is also shown in the bottom panel. The supercooled liquid water depth W is shown in the top panel. The arrows in the middle panel show, at the Omegasonde launch times, the mean wind speed and direction in the cloud layer calculated to contain the supercooled liquid water. [For reference, a small map of Baw Baw Plateau (contours at 1000 m MSL) is shown at the right-hand end of the line of arrows. Note that a southwesterly wind is perpendicular to the long axis of the plateau and a northwesterly wind is parallel to this axis.]

The local atmospheric structure in Fig. 6 is defined by Omegasondes launched during the storm. Tick marks along the upper side of the abscissa show when the Omegasondes were launched. The horizontal line near 840 mb shows the height of the radiometer.

Two frontal zones are shown in Figs. 6a,b. They are derived from equivalent potential temperature (Fig. 6a) and analysis of wind and temperature (Fig. 6b). The zones were embedded in the leading sides of troughs and preceded the trough axes by 6–9 h.

There is an association of the two main precipitation-flux maxima in the storm in Fig. 5 with the two frontal zones. These precipitation-flux maxima occurred at 1900 LST 5 August and at 1200 LST 7 August.

A comparison of the precipitation flux and supercooled liquid water flux during the storm is as follows. During the two frontal zones, the precipitation flux reached peaks (~ 1 h wide) of 1200 and 1100 MI h^{-1} (2.4 and 2.2 mm h^{-1}), respectively. The supercooled liquid water flux peaks were 3–4 h wide and of magnitude 200 and 1400 MI h^{-1} (0.4 and 2.8 mm h^{-1}), respectively.

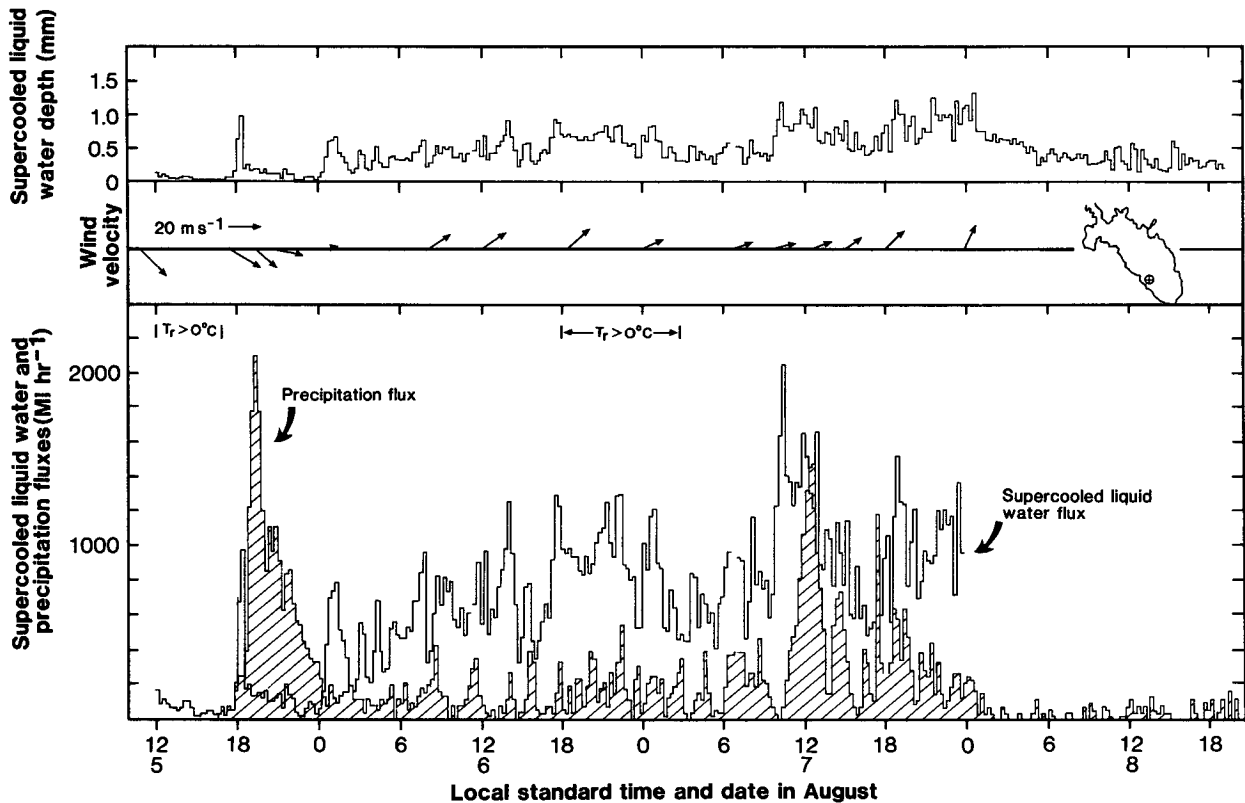


FIG. 5. Bottom panel shows time series, at 15-min intervals on 5–8 August 1988, of mean precipitation flux a_2 (MI h^{-1}) (hatched histogram) over target area and of supercooled liquid water flux a_2 (MI h^{-1}) (plain histogram) across Baw Baw Plateau and adjoining mountain ridge upwind of target area. Marked intervals $T_r > 0^\circ\text{C}$ show times when temperature at radiometer was greater than 0°C . Top panel shows time series, at same 15-min interval, of radiometric supercooled liquid water depth W . Middle-panel arrows show average direction and speed of wind in layer of cloud containing supercooled liquid water.

In the first frontal zone the supercooled liquid water flux was approximately 0.2 of and 1000 MI h^{-1} less than the precipitation flux. This suggests little potential increase in the precipitation flux by seeding. In the second frontal zone the supercooled liquid water flux was approximately 1.3 times the precipitation flux and exceeded the precipitation flux by 300 MI h^{-1} , and there was a large potential increase in precipitation flux by seeding.

The ratios of 0.2 and 1.3 can be compared with the results of others quoted in section 1. The smaller value obtained here is typical of these earlier results. The larger value exceeds those results and suggests that there may be larger potential artificial increase in precipitation than heretofore estimated for winter storm clouds in mountainous regions.

It is worthwhile considering the conditions under which the supercooled liquid water flux was low and high relative to the precipitation flux in the first and second frontal zone.

The hypothesis for the lower supercooled liquid flux rather than precipitation flux in the first frontal zone is connected with the wind direction and the orientation of the orography. In particular, the wind was

northwesterly ($300^\circ\text{--}320^\circ$) (see Fig. 6b) and the Baw Baw Plateau was oriented with its end in the upwind direction. Section 5 shows that for such a *northwesterly wind* the magnitude of the supercooled liquid water flux (as plotted in Fig. 5) should have been lower than existed at the boundary point. This lower magnitude is treated as an observational error associated with the physical displacement of the radiometer site from the boundary point. The supercooled liquid water flux should thus have actually been greater than shown near frontal zone 1 in Fig. 5.

During the second frontal zone, the supercooled liquid water flux was greater than the precipitation flux. This occurred when the wind was from the southwest (see Fig. 6b) and orthogonally impacting the main frontal face of the plateau at 20 m s^{-1} (see Fig. 5) with hypothesized maximum lift, condensation, and liquid water development. Extrapolation of the radiometer supercooled liquid water depth to the boundary point again occurred in constructing Fig. 5, as it did for frontal zone 1, but the extrapolation was over a short, 9-km distance, along Baw Baw Plateau. The extrapolation error in the supercooled liquid water depth was expected to be small (see section 5). The comparison

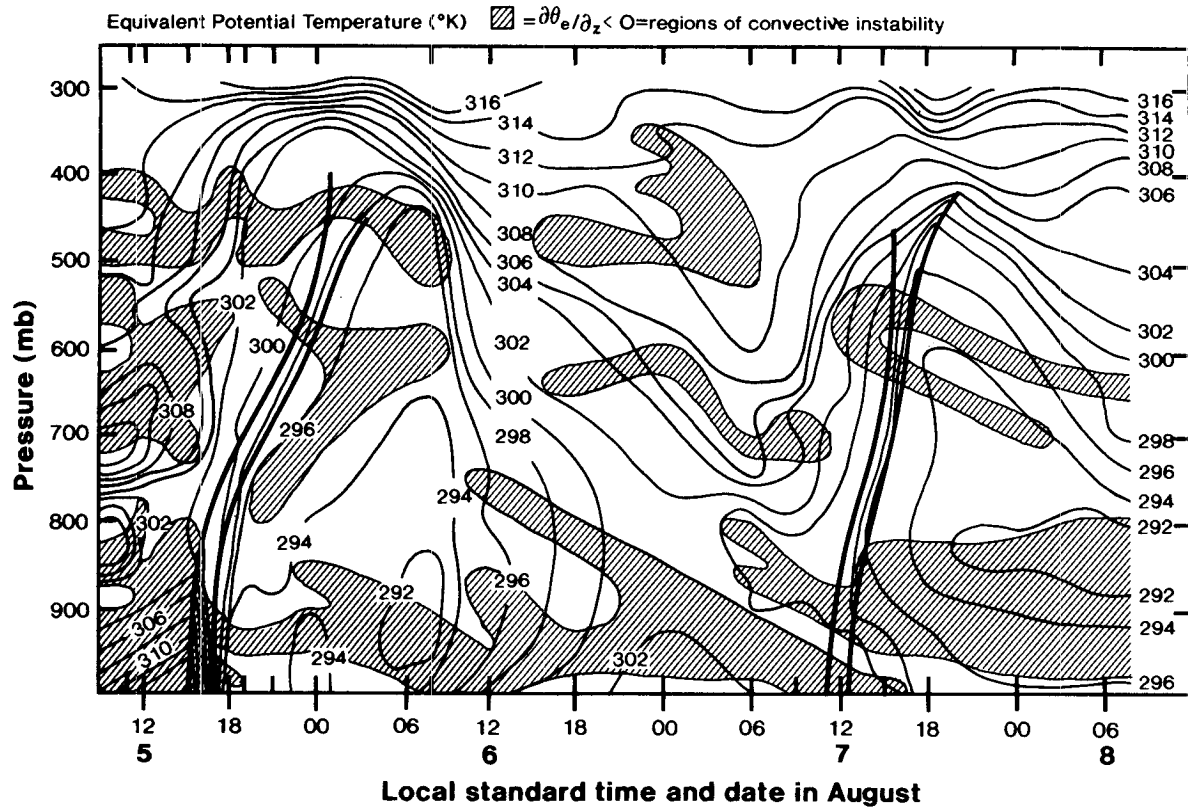


FIG. 6a. Contoured plot of equivalent potential temperature as a function of local time and pressure-altitude on 5–8 August 1988 and as measured with Omegasondes.

of the relatively large supercooled liquid water flux with the smaller precipitation flux is expected to be accurate. It indicates potentially suitable conditions for precipitation enhancement activities.

During the time in the storm between the two frontal zones (0000 LST 6 August–0900 LST 7 August) the supercooled liquid water flux was significantly greater than the precipitation flux. The supercooled liquid water flux was approximately 600 MI h^{-1} , or three times as high as the precipitation flux of about 200 MI h^{-1} . The excess flux suggests suitable conditions for seeding. The condition described previously, of southwesterly flow orthogonal to the plateau with maximum lift and condensation, accompanying significant amounts of supercooled liquid water during the second frontal passage, also was obtained during much of the period between fronts discussed in this paragraph. This condition is offered as a hypothetical explanation for the general validity of the large supercooled liquid water fluxes observed between the fronts.

The temporal variability of the supercooled liquid water flux in between the frontal zones in Fig. 5 is attributed to two factors. Slow-changing synoptic-scale controls are responsible for the gradual changes of the supercooled liquid water flux over long (e.g., 12–18 h) subintervals between the fronts. These controls may be large-scale lifting motions or changes in the atmo-

spheric vapor content and saturation state. Also shown in Fig. 5 are more rapid changes in the supercooled liquid water and precipitation fluxes, on a scale of 1–2 h. They are attributed to smaller mesoscale updrafts and concentrations of supercooled liquid water. Mesoscale structures in the context of weather modification have been discussed recently by Huggins et al. (1989), Long et al. (1990), and Sassen et al. (1990).

Subsequent to the second front there were 15 h when the supercooled liquid water flux exceeded the precipitation flux. The mean supercooled liquid water flux was 700 MI h^{-1} , or 2.3 times the precipitation flux of 300 MI h^{-1} . Conditions were potentially suitable for precipitation-enhancement activities. During the time period of these results, the flow was southwest to south-southwest, and significant lift and condensation were expected over Baw Baw Plateau.

This section has shown that storm 1 was important from the standpoint of precipitation enhancement. In the period between the fronts, during the second frontal zone, and in the period after the second front, winds were southwesterly. Between the fronts the precipitation flux was 200 MI h^{-1} , while the supercooled liquid water flux was 600 MI h^{-1} . In the second frontal zone the precipitation flux was 1100 MI h^{-1} . Supercooled liquid water flux was larger (1400 MI h^{-1}). After the second front, the precipitation flux was 300 MI h^{-1} ,

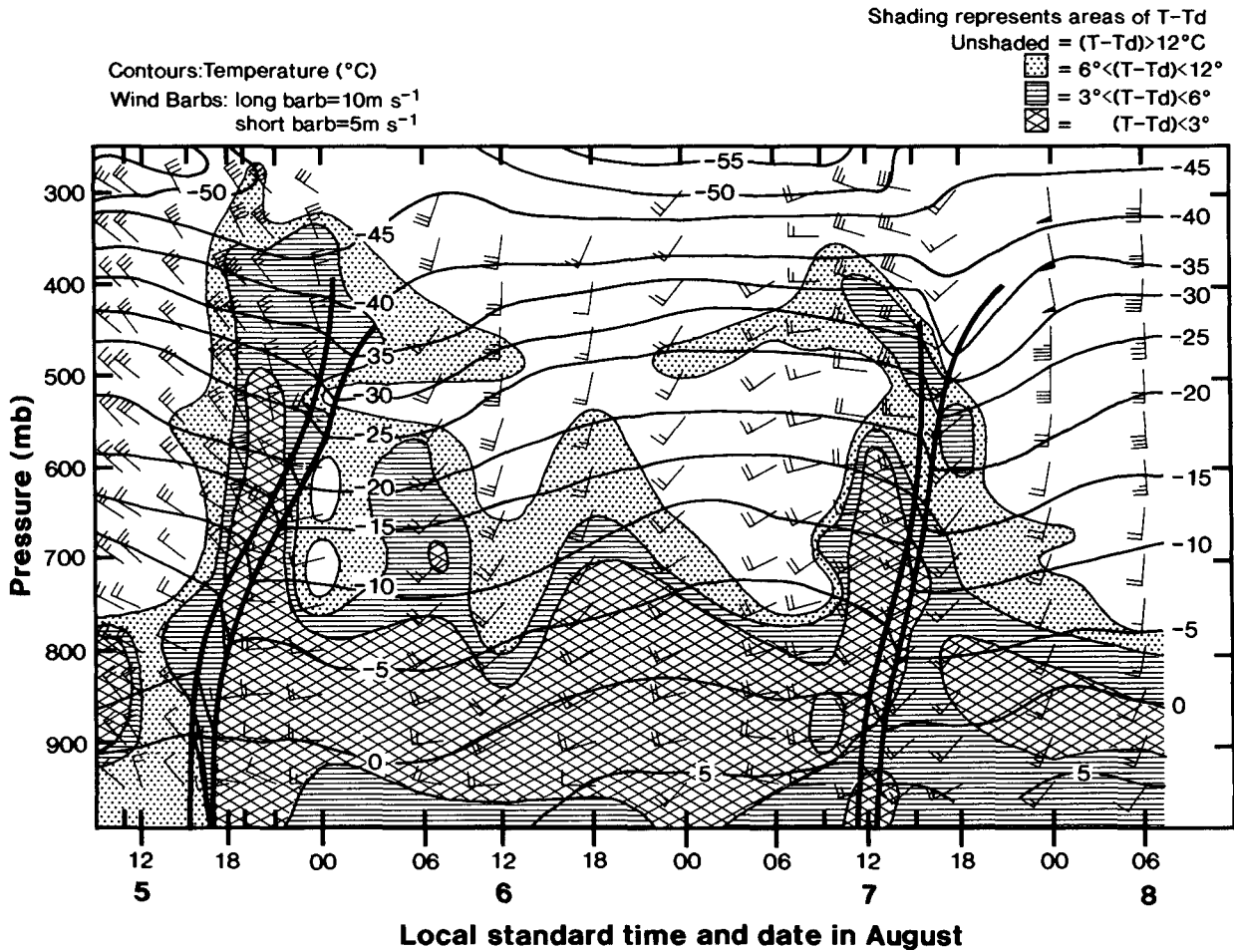


FIG. 6b. Plot of wind velocity, temperature, and dewpoint depression as a function of local time and pressure-altitude on 5-8 August 1988 and as measured with Omegasondes.

while the supercooled liquid water flux was 700 MI h^{-1} . Cloud-top temperatures were warm at -5° to -10°C between the fronts and subsequent to the second front. The results overall suggest that the periods of southwesterly flow between the fronts and postfrontally were the best suited for precipitation enhancement activity.

7. Storm 2: 24-27 July 1988

Figure 7 graphically displays the same kind of information for this storm as Fig. 5 displayed for storm 1 in section 6.

During the first stage of the storm two fronts passed. With the first front, from 0800 to 1400 LST 25 July, precipitation and supercooled liquid water fluxes of similar magnitude (1100 MI h^{-1} and 900 MI h^{-1} , respectively) were observed. With the second front from 1500 to 1800 LST 25 July, the precipitation flux was typically 1200 MI h^{-1} . The supercooled liquid water flux was about 800 MI h^{-1} . During the period of these fronts the winds were from 280° to 300° at $30\text{--}35 \text{ m s}^{-1}$.

Following the passage of the second cold front at 1800 LST 25 July there was backing of the wind at most altitudes from about 290° to 220° at 0000 LST 27 July. The wind was from the southwest and orthogonal to the plateau with expected significant condensation and liquid water formation. During most of this period cloud tops were relatively cold. Only from 1500 LST 26 July to 0200 LST 27 July were cloud-top temperatures greater than -10°C and warm enough for the natural precipitation process to be inefficient and for precipitation enhancement to have an opening for success. From 1800 LST 25 July to 0600 LST 27 July the supercooled liquid water flux was 1200 MI h^{-1} , while the precipitation flux was only 300 MI h^{-1} . A good opportunity for seeding was available in the late postfrontal stage of this storm.

8. Storm 3: 26-28 August 1988

This section discusses the supercooled liquid water and precipitation fluxes for storm 3. Reference is made to Fig. 8.

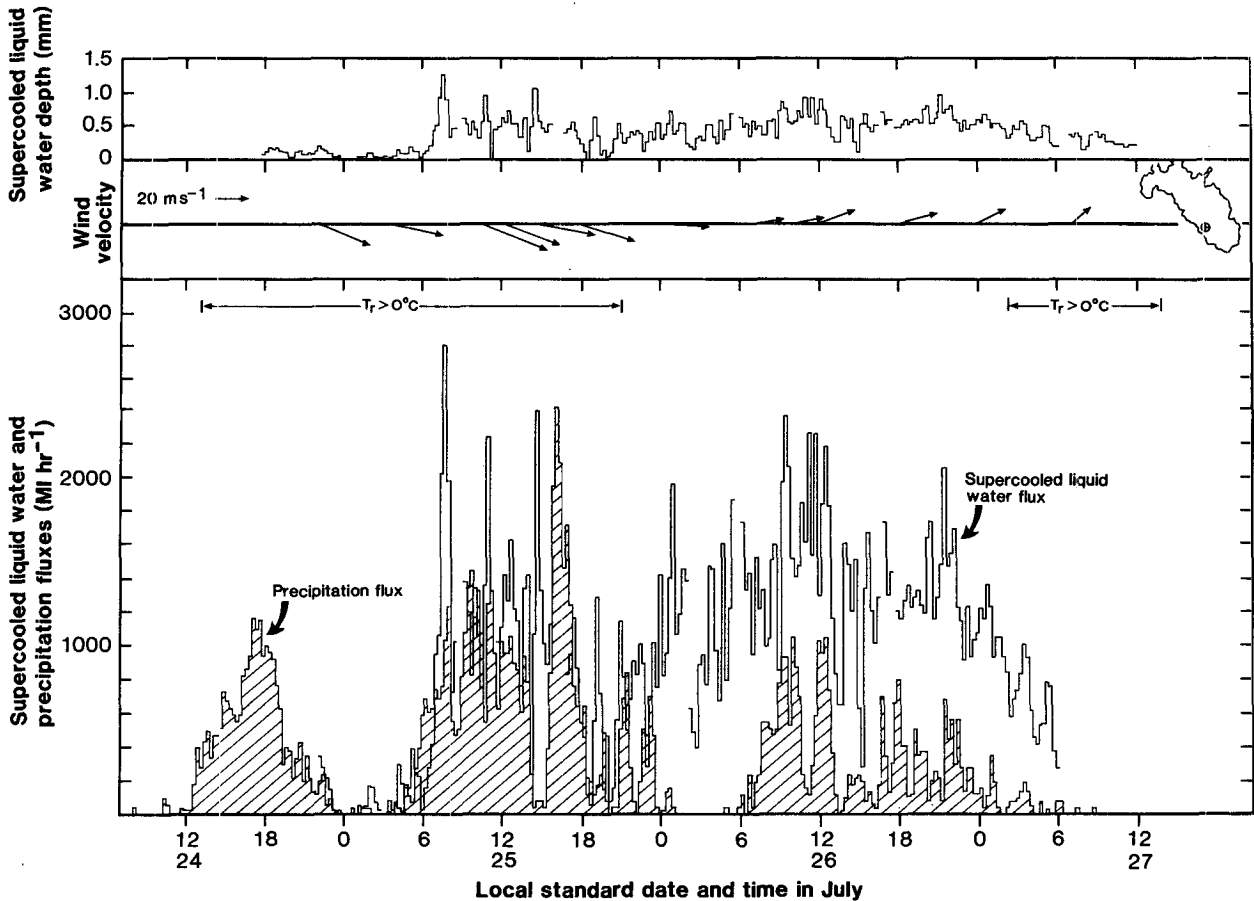


FIG. 7. Same as Fig. 5, but for 24–27 July 1988.

During the frontal-zone period from 1300 to 1700 LST 27 August, the precipitation flux reached 1400 MI h^{-1} while the supercooled liquid water flux did not exceed 100 MI h^{-1} .

Winds were from the northwest and light at about 12 m s^{-1} . Orographic lift by the plateau would have been minimal, and this may explain the small, supercooled liquid water flux that was observed. During the frontal passage cloud-top temperatures were about -20°C . This and the large precipitation flux suggest an efficient precipitation process.

In the initial postfrontal period, from 1700 to 2300 LST 27 August, the supercooled liquid water flux averaged 600 MI h^{-1} and was larger than the precipitation flux (of 400 MI h^{-1}) for the first time in the storm. The greater supercooled liquid water flux is attributed to (a) backing of the wind, at 850–500 mb, from 300° – 320° to 240° and almost orthogonal to Baw Baw Plateau and (b) a wind-speed increase from 12 to 15 m s^{-1} . From 2300 LST 27 August to 2100 LST 28 August, the wind continued to be favorable and the supercooled liquid water flux was still about 600 MI h^{-1} and consistently greater than the precipitation flux of 300 MI h^{-1} . The cloud-top temperature was -10°C or warmer in the postfrontal period. This observation and

the low precipitation flux suggest an inefficient precipitation process. The higher supercooled liquid water flux and the warmer, less efficient clouds suggest that this was an appropriate time for precipitation-enhancement activity in this storm.

9. Conclusions

An important result of this paper has been the magnitudes of (a) the supercooled liquid water flux across the upwind boundary of the target area and (b) the precipitation flux over the project target area. The supercooled liquid water flux has been viewed as the maximum potential increase in the precipitation flux that may result from cloud seeding.

Table 1 lists the average magnitudes of these variables for several periods of similar meteorology in the three winter storms considered here.

Three of the five cold-frontal periods (storm periods 1, 6, and 8 in Table 1) produced a supercooled liquid water to precipitation-flux ratio that was less than 1. This occurred with northwesterly to west-northwesterly winds. This result was due, we believe, to a relatively efficient conversion of cloud water to precipitation within the relatively deep and cold-topped (-15° to

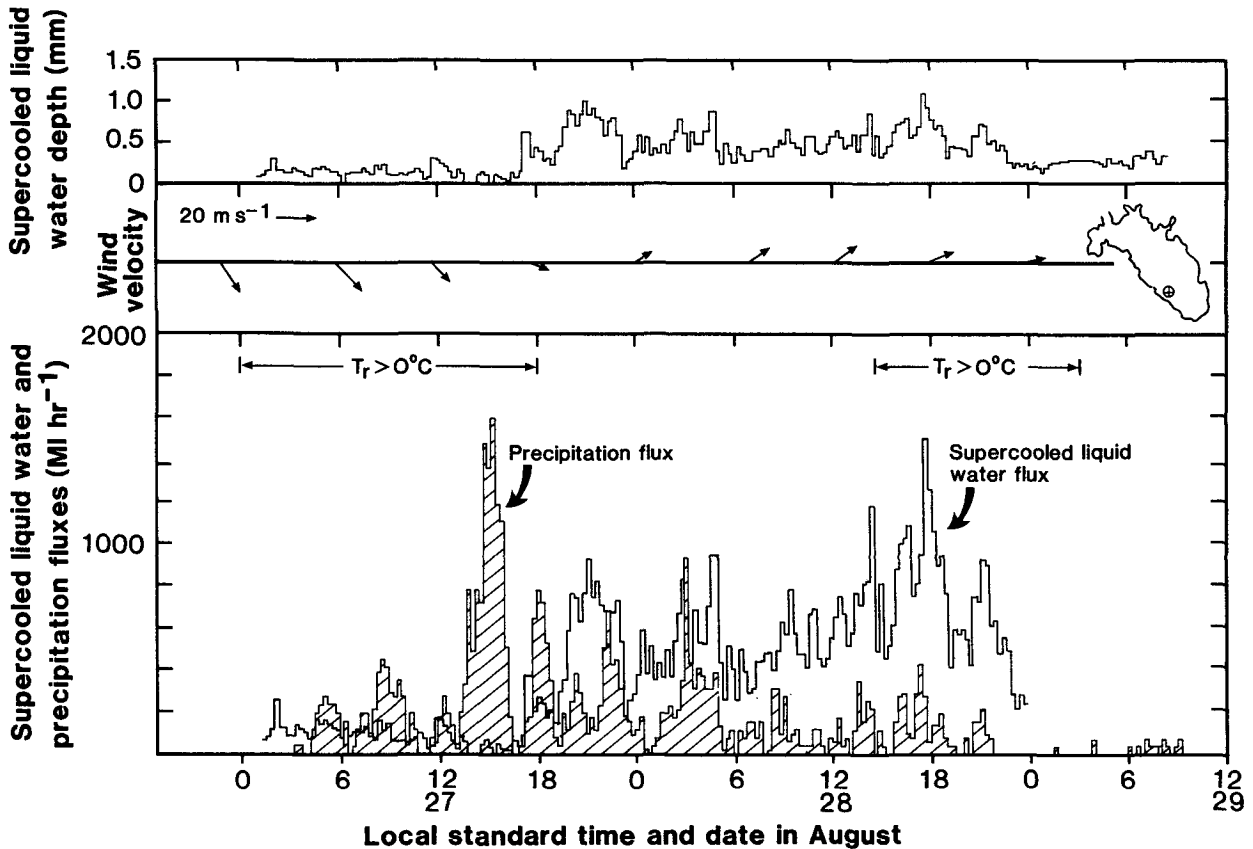


FIG. 8. Same as Fig. 5, but for 27–29 August 1988.

−29°C) clouds accompanying these fronts. The flux ratios were less than 1 perhaps also because of the possibility that the supercooled liquid water flux was underestimated in conditions of northwest winds. This would have been due to the radiometric measurements being made on the southwest face of the plateau, where orographic lift and condensation in northwesterly flow would have been minimal—being used to approximate the liquid water on the northwest end of the plateau.

For two of the five cold-frontal periods (storm periods 3 and 5) the supercooled liquid water to precipitation-flux ratio was equal to or slightly greater than 1. One period (period 3) occurred in southwesterly

flow where a greater cross-barrier wind speed and subsequent orographic lift would have produced a larger supercooled cloud-water flux. The other front (period 5), though occurring with west-northwesterly winds, had extremely strong (30–35 m s^{−1}) winds and thus a cross-barrier component sufficient to produce significant amounts of orographically induced cloud water, in contrast to the three earlier fronts (1, 6, and 8) that produced only a little cloud water. Obviously, the variable interaction of fronts with the plateau can lead to a variable supercooled liquid water flux and a variable ratio between this flux and the precipitation flux.

The four periods (periods 2, 4, 7, and 9) representing

TABLE 1. Comparison of precipitation, d_2 , and supercooled liquid water, a_2 , fluxes.

Storm period	Storm number	Period definition	Time period (CST)	d_2 (MI h ^{−1})	a_2 (MI h ^{−1})	a_2/d_2	Wind direction
1	1	First cold front	1800–2200 5 Aug	1200	200	0.2	NW
2	1	Between fronts	0100 6 Aug–0900 7 Aug	200	600	3.0	SW/WSW
3	1	Second cold front	0900–1300 7 Aug	1100	1400	1.3	SW/WSW
4	1	Postfrontal	1300 7 Aug–0600 8 Aug	300	700	2.3	SW/SSW
5	2	First cold front	0800–1400 25 Jul	1100	900	1.0	NW/WNW
6	2	Second cold front	1600–1800 25 Jul	1200	800	0.7	WNW
7	2	Postfrontal	1800 25 Jul–0900 27 Jul	300	1200	4.0	W/WSW
8	3	Cold front	1300–1600 27 Aug	1400	100	0.1	NW/WNW
9	3	Postfrontal	1700 27 Aug–2100 28 Aug	300	600	2.0	SW

predominantly postfrontal conditions exhibited supercooled liquid water to precipitation-flux ratios consistently and significantly greater than 1. Here the cloud liquid water flux was maximized by vertical lift from southwesterly airflow that was normal to the plateau barrier. The precipitation flux was lower than for frontal periods. This is attributed to lower, warmer cloud tops with a less efficient precipitation process. Overall, the postfrontal periods appear to represent a greater potential for precipitation enhancement than do frontal periods. It should be noted that the ratios a_2/d_2 during the postfrontal period are significantly greater than the ratios (all less than 0.5) found by Heggli (1986), Rauber and Grant (1987), and Super and Boe (1988a). This may be because runoff data averaged over a long period of time were used by these workers. The present results over shorter time periods suggest there can be a larger potential increase in precipitation for winter storm clouds in mountainous regions.

The cloud-top temperature is a variable usually discussed in precipitation-enhancement studies. In the present study it has been of secondary interest behind fluxes of condensed water substance. Nevertheless, in the storms treated here, there were significant periods of warm cloud-top temperatures, of -5° to -10°C , that are important in precipitation enhancement. In storm 1, such temperatures were observed for 22 h. In storm 2 the figure was 7 h, and in storm 3 the figure was 24 h. Most of these temperatures occurred in the postfrontal stages of the storms when seeding opportunities were greatest from the standpoint of large water-flux ratios.

This paper has made some progress toward two research objectives. *First*, estimates have been made of the horizontal flux of supercooled liquid water across the upwind boundary of the target area of the MMBW precipitation-enhancement experiment. This horizontal flux is frequently greater than the vertical precipitation flux downwind in the target area. It has been assumed that the horizontal flux is an upper bound on the increase in vertical precipitation mass flux, which may result from cloud seeding. The horizontal- and vertical-flux measurements supporting these results were made with appropriate ground, in situ, and remote-sensing instruments. The errors in these measurements were discussed.

Second, the meteorological circumstances associated with the horizontal supercooled liquid water fluxes, which were favorably and particularly large compared to precipitation fluxes, have been determined. The circumstances are a postfrontal, southwesterly wind orthogonal to Baw Baw Plateau along the upwind boundary of the target area. Observations were also made of warm cloud tops ($T > -10^\circ\text{C}$). These circumstances have been found to apply in three different winter storms. Overall, more definite knowledge is now available about the circumstances under which cloud seeding may be conducted with advantage.

A positive difference of $400\text{--}800 \text{ MI h}^{-1}$ was frequently found between the postfrontal supercooled liquid water and precipitation fluxes. Since a typical valuation of this water is \$A100–400 per megaliter, it is seen that even a modest increase of precipitation, by seeding the horizontally flowing supercooled liquid water, will more than pay for the cost of the seeding and, in general, be valuable.

Acknowledgments. Assistance with this research has come from a number of individuals. At the CSIRO Division of Atmospheric Research (DAR), Ronald Hill and Reg Henry provided logistics support in setting up the remote-sensing instrumentation and installing extra precipitation gauges. Sunhee Lee assisted with computer processing of the radiometer and Omegasonde data. Sean Higgins and Louise Carr produced the graphics.

At the Melbourne and Metropolitan Board of Works (MMBW), Robert Dorrat was the primary liaison between the DAR and the MMBW. Ian Searle, John Barry-Murphy, and Peter Murphy provided weather information from the MMBW cloud-seeding experiment. Levente Szirom provided precipitation data from the MMBW experiment.

At the Bureau of Meteorology, Graham Duff, Colin Irvine, and Julie Matthews operated the Omegasonde equipment and provided processed data.

Richard Smith of the Desert Research Institute installed and operated the microwave radiometer.

Toyota provided 4-wheel-drive vehicles, and QANTAS provided airfares between the United States and Australia.

This research was supported in part by the Melbourne and Metropolitan Board of Works and in part by the U.S. National Science Foundation Division of Atmospheric Sciences under Grants ATM-8603089 and ATM-8812302.

REFERENCES

- Boe, B. A., and A. B. Super, 1986: Wintertime characteristics of supercooled liquid water over the Grand Mesa of western Colorado. *J. Wea. Mod.*, **18**, 102–107.
- Fraser, D. A. S., 1958: *Statistics—An Introduction*. John Wiley and Sons, 114–119 pp.
- Heggli, M., 1986: A ground-based approach used to determine cloud seeding opportunity. Preprints, *Tenth Conf. on Weather Modification*, Arlington, VA, Amer. Meteor. Soc., 64–67.
- , R. M. Rauber, and J. B. Snider, 1987: Field evaluation of a dual-channel microwave radiometer designed for measurements of integrated water vapor and cloud liquid water in the atmosphere. *J. Atmos. Oceanic Technol.*, **4**, 204–213.
- Hogg, D. C., F. O. Guiraud, J. B. Snider, M. T. Decker, and E. R. Westwater, 1983: A steerable dual-channel microwave radiometer for measurement of water vapor and liquid in the troposphere. *J. Climate Appl. Meteor.*, **22**, 789–806.
- Huggins, A. W., A. B. Long, and B. Campistron, 1989: The impact of mesoscale precipitation bands on liquid water and precipitation efficiency in a winter mountain storm in Utah. *Fifth WMO Scientific Conf. on Weather Modification and Applied Cloud Physics*, Beijing. World Meteorological Organization, 55–58.

- Long, A. B., and D. E. Shaw, 1988: Design of a precipitation augmentation experiment for the MMBW Thomson Reservoir catchment. Tech. Rep. to Melbourne and Metropolitan Board of Works, 93 pp. [Available from Melbourne and Metropolitan Board of Works, Melbourne.]
- , B. A. Campistron, and A. W. Huggins, 1990: Investigations of a winter mountain storm in Utah. Part I: Synoptic analysis, mesoscale kinematics, and water release rates. *J. Atmos. Sci.*, **47**, 1302–1322.
- Rauber, R. M., and L. O. Grant, 1986: The characteristics and distribution of cloud water over the mountains of northern Colorado during wintertime storms. Part II: Spatial distribution and microphysical characteristics. *J. Climate Appl. Meteor.*, **25**, 489–504.
- , and ———, 1987: Supercooled liquid water structure of a shallow orographic cloud system in southern Utah. *J. Appl. Meteor.*, **26**, 208–215.
- Sassen, K., A. W. Huggins, A. B. Long, J. B. Snider, and R. J. Meitin, 1990: Investigations of a winter mountain storm in Utah. Part II: Mesoscale structure, supercooled liquid water development, and precipitation processes. *J. Atmos. Sci.*, **47**, 1323–1350.
- Super, A. B., and B. A. Boe, 1988a: Wintertime cloud liquid water observations over the Mogollon Rim of Arizona. *J. Wea. Mod.*, **20**, 1–8.
- , and ———, 1988b: Microphysical effects of wintertime cloud seeding with silver iodide over the Rocky Mountains. Part III: Observations over the Grand Mesa, Colorado. *J. Appl. Meteor.*, **27**, 1166–1182.
- , and J. A. Heimbach, Jr., 1988: Microphysical effects of wintertime cloud seeding with silver iodide over the Rocky Mountains. Part II: Observations over the Bridger Range, Montana. *J. Appl. Meteor.*, **27**, 1152–1165.
- Thompson, J. R., and A. B. Super, 1987: Wintertime supercooled liquid water flux over the Grand Mesa, Colorado. *J. Wea. Mod.*, **19**, 92–98.